

# TIRF microscopy analysis of human Cof1, Cof2, and ADF effects on actin filament severing and turnover

Samantha M. Chin, Silvia Jansen and Bruce L. Goode

Department of Biology, Rosenstiel Basic Medical Science Research Center, Brandeis University, Waltham, MA 02454, USA

**Correspondence to Bruce L. Goode:** Rosenstiel Basic Medical Science Research Center, Brandeis University, 415 South St., Waltham, MA 02454, USA. [goode@brandeis.edu](mailto:goode@brandeis.edu)

<http://dx.doi.org/10.1016/j.jmb.2016.03.006>

Edited by James Sellers

## Abstract

Dynamic remodeling and turnover of cellular actin networks requires actin filament severing by actin-depolymerizing factor (ADF)/Cofilin proteins. Mammals express three different ADF/Cofilins (Cof1, Cof2, and ADF), and genetic studies suggest that *in vivo* they perform both overlapping and unique functions. To gain mechanistic insights into their different roles, we directly compared their G-actin and F-actin binding affinities, and quantified the actin filament severing activities of human Cof1, Cof2, and ADF using *in vitro* total internal reflection fluorescence microscopy. All three ADF/Cofilins had similar affinities for G-actin and F-actin. However, Cof2 and ADF severed filaments much more efficiently than Cof1 at both lower and higher concentrations and using either muscle or platelet actin. Furthermore, Cof2 and ADF were more effective than Cof1 in promoting “enhanced disassembly” when combined with actin disassembly co-factors Coronin-1B and actin-interacting protein 1 (AIP1), and these differences were observed on both preformed and actively growing filaments. To probe the mechanism underlying these differences, we used multi-wavelength total internal reflection fluorescence microscopy to directly observe Cy3–Cof1 and Cy3–Cof2 interacting with actin filaments in real time during severing. Cof1 and Cof2 each bound to filaments with similar kinetics, yet Cof2 induced severing much more rapidly than Cof1, decreasing the time interval between initial binding on a filament and severing at the same location. These differences in ADF/Cofilin activities and mechanisms may be used in cells to tune filament turnover rates, which can vary widely for different actin structures.

© 2016 The Authors. Published by Elsevier Ltd. This is an open access article under the CC BY-NC-ND license (<http://creativecommons.org/licenses/by-nc-nd/4.0/>).

## Introduction

Actin-depolymerizing factor (ADF)/Cofilin proteins are a family of actin severing proteins that are expressed in all plant, animal, and fungal species and play essential roles in driving dynamic turnover of the actin cytoskeleton in a wide range of cellular and physiological processes [1–4]. Simple model organisms such as *Saccharomyces cerevisiae*, *Drosophila melanogaster*, and *Dictyostelium discoideum* have a single Cofilin gene that is essential for viability [5–8]. However, mammals have three separate ADF/Cofilin genes, from which they express three different proteins: Cofilin-1, Cofilin-2, and ADF (hereafter referred to as Cof1, Cof2, and ADF). Most non-muscle cell and tissue types express both Cof1 and ADF, but at different

levels, and some cell types express all three ADF/Cofilins [9–13]. Cof2 is found primarily in muscle, but also in the brain and liver [9], and in oligodendrocytes and keratinocytes [12,13]. Genetic studies suggest that the three ADF/Cofilins have distinct physiological roles. In mice, a Cof1<sup>-/-</sup> knockout is embryonic lethal [14], whereas an ADF<sup>-/-</sup> knockout leads to corneal thickening and blindness, and a Cof2<sup>-/-</sup> knockout causes severe disruption of muscle architecture and post-natal lethal cardiomyopathies [15,16]. Additional genetic insights into ADF/Cofilin isoform function have come from silencing studies in cultured cells. Several groups have shown that depletion of Cof1 impairs directed cell migration, and that these defects can only be rescued by Cof1 and not ADF [10,11,17,18]. Collectively, these observations indicate that while

the three ADF/Cofilins may have some overlapping functions, they also perform unique roles *in vivo*.

*In vitro* studies on ADF/Cofilins have shown that they bind G-actin and F-actin, and exhibit a strong preference for actin in the ADP-bound rather than ATP- or ADP + P<sub>i</sub>-bound states [1,19,20]. ADF/Cofilins bind to G-actin between subdomains I and III, and strongly inhibit nucleotide exchange on actin monomers [21]. Real-time imaging using multi-wavelength total internal reflection fluorescence (TIRF) microscopy has shown that yeast Cofilin and human Cof1 bind actin filaments in a cooperative manner and induce severing at the boundaries between bare and decorated segments [22–24]. ADF/Cofilin binding also alters the structure and mechanical properties of actin filaments [21,22,25–29] and induces the release of cations to “soften” F-actin, creating mechanical discontinuities that induce fragmentation [27]. On the other hand, over-decoration leads to filament stabilization [30]. Other studies have shown that severing by ADF/Cofilins can be greatly enhanced by cellular co-factors. For both yeast Cofilin and human Cof1, Coronin has been shown to enhance their severing activities by altering F-actin structure and/or accelerating their recruitment to filament sides [24,31]. In contrast, suppressor of Ras<sup>Val19</sup>/cyclase-associated protein (Srv2/CAP) and actin-interacting protein 1 (AIP1) enhance yeast Cofilin and human Cof1 severing without altering their kinetics of recruitment to filament sides [23,24,32–35]. To date, these *in vitro* mechanistic TIRF studies on Cofilin have been limited to yeast and human Cof1, leaving open the question of whether the other mammalian ADF/Cofilins have similar or distinct activities, and whether their activities are similarly enhanced by these co-factors.

Earlier studies using bulk fluorescence assays and electron microscopy to measure filament fragmentation and disassembly reported that ADF has a stronger disassembly-promoting activity than Cof1 [36]. However, a different study using F-actin sedimentation reported that ADF and Cof1 have similar disassembly activities, and that Cof2 is less active than ADF and Cof1 [9]. Yet another study from the same group later used bulk pyrene-F-actin depolymerization assays and reported that Cof1 and Cof2 have similar kinetic effects on disassembly [37]. Thus, there have been conflicting reports about the relative efficiencies of Cof1, Cof2, and ADF in promoting severing and disassembly, with some of this variability likely arising from the specific techniques used and the caveats associated with those methods.

Here, we directly compared the G-actin and F-actin binding affinities of human Cof1, Cof2, and ADF and then used *in vitro* TIRF microscopy analysis to directly observe in real time and rigorously quantify their severing activities. To our knowledge, no study to date has compared the activities of the three ADF/Cofilins by this powerful approach. Our analysis has revealed key differences

in their severing activities and mechanisms, which offer new insights into how cells may differentially deploy these three proteins to tune actin network turnover.

## Results

### Human Cof1, Cof2, and ADF have similar binding affinities for G-actin and F-actin

Common properties of ADF/Cofilins are their ability to bind F-actin and their ability to bind actin monomers and inhibit the conversion of ADP-G-actin to ATP-G-actin [38–40]. As a first step in testing the similarities and differences in human Cof1, Cof2, and ADF activities, we directly compared their effects on ADP-G-actin in nucleotide exchange assays. Over a wide concentration range, Cof1, Cof2, and ADF showed similar effects ( $K_{app}$ ) in reducing the rate of  $\epsilon$ -ATP exchange on ADP-G-actin (Fig. 1a–c), in good agreement with a previous study that directly compared Cof1 and ADF [36]. In addition, we used pyrene-quenching assays [41,42] to directly compare the F-actin binding affinities ( $K_d$ ) of Cof1, Cof2, and ADF. Our results showed that all three ADF/Cofilins bind with similar affinity to F-actin (Fig. 1d–f). Thus, there appear to be only minor differences in the G-actin and F-actin binding affinities of Cof1, Cof2, and ADF.

### Cof2 and ADF sever filaments more efficiently than Cof1 under multiple conditions

Next we compared the actin filament severing activities of the three ADF/Cofilins in TIRF microscopy assays, where severing events could be observed in real time. Initially, we compared ADF/Cofilin effects on preformed actin filaments. Fluorescently labeled filaments [10% Oregon Green (OG)-actin; 0.5% biotin-actin] were polymerized and sparsely tethered to the viewing surface. Then actin monomers were flowed out, and Cof1, Cof2, or ADF was flowed in (Fig. 2a and Movie S1). Based on known rate constants for ATP hydrolysis and Pi release [43,44], these pre-assembled filaments consist predominantly of ADP-bound actin subunits by the time of flow-in. At first, we used 1  $\mu$ M ADF/Cofilin in these assays, since a number of previous studies compared ADF/Cofilin effects on actin disassembly at similar concentrations [9,36]. Under these conditions, we observed rapid severing, with measurable cumulative severing reaching a plateau after 20–50 s (Fig. 2b). Further analysis of these data showed that the time to half-maximal severing was significantly longer for Cof1 compared to Cof2 and ADF (Fig. 2c;  $T_{1/2}$  of 15.2, 5.5, and 8.4 s, respectively). Thus, at these higher concentrations

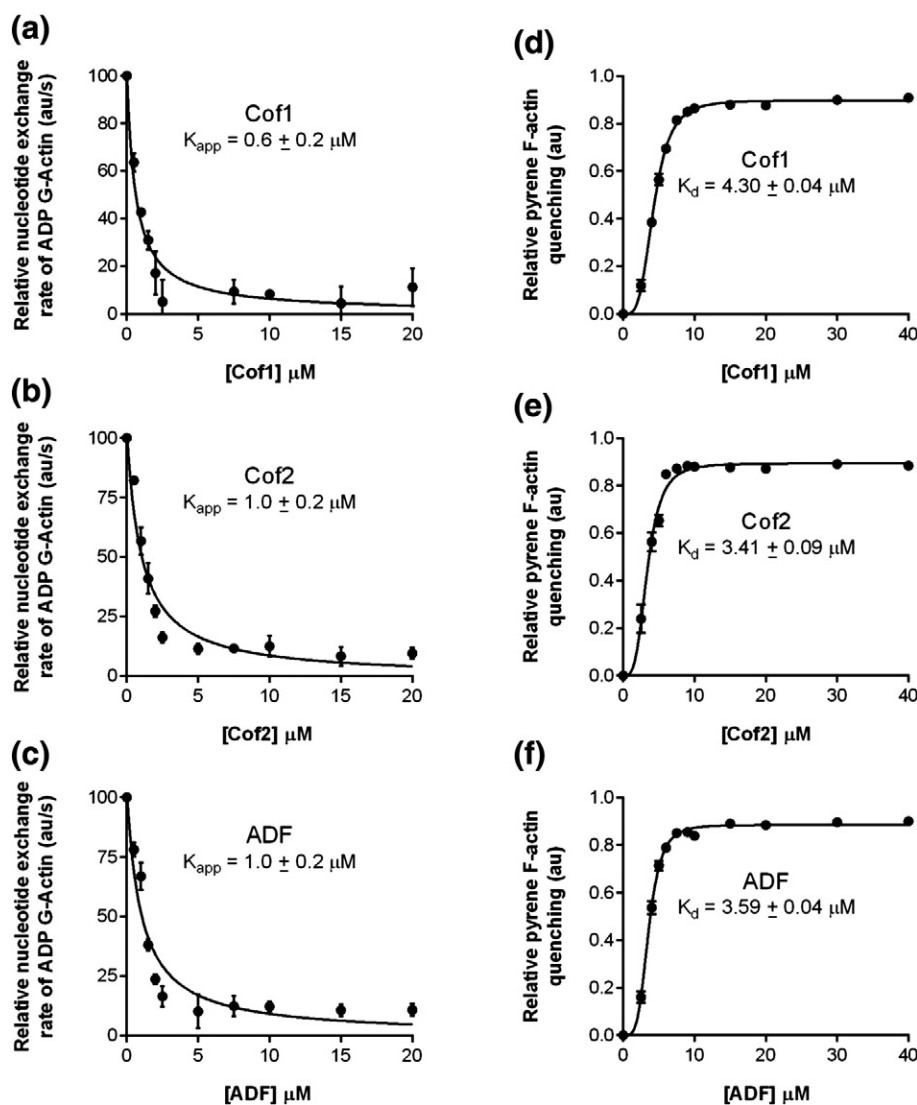


**Fig. 1.** Cof1, Cof2, and ADF bind to G-actin and F-actin with similar affinities. (a–c) Nucleotide exchange rate on 2 μM ADP-actin monomers in the presence of different concentrations of the ADF/Cofilin indicated. Each data point on the graph is the average from three independent trials. Data were fit to the equation  $f = y_0 - ax/(b + x)$  to determine  $K_{app}$ . (d–f) Pyrene quenching of 2 μM pre-assembled F-actin in the presence of different concentrations of Cof1, Cof2, or ADF. Each data point on the graph is the average from three independent trials. Data were fit to the equation  $f = (B_{max} * x^h)/(K_d^h + x^h)$  to determine the  $K_d$ . Error bars represent SEM.

(1 μM), Cof2 and ADF sever filaments more efficiently than Cof1.

To enable more accurate quantification of severing and thus more accurate comparison of differences in severing efficiency, we next compared activities at a lower concentration (150 nM) of ADF/Cofilin proteins. Again, even though the concentration was approximately sevenfold lower, the same trend was observed; that is, Cof2 and ADF severed filaments more efficiently than Cof1 (Fig. 2e and f; Movie S2). More specifically, times to half-maximal severing ( $T_{1/2}$ ) were approximately sixfold and fourfold

shorter for Cof2 and ADF compared to Cof1, respectively (Fig. 2g). Thus, at both higher and lower concentrations, Cof2 and ADF have substantially stronger severing activities than Cof1.

At lower concentration (150 nM), the ADF/Cofilins induced about twice as many cumulative severing events per μm filament compared to at higher concentrations (compare plateaus in Fig. 2b and f). However, it took longer to reach maximal cumulative severing at the lower concentrations of ADF/Cofilin. These results can be explained by the known properties of ADF/Cofilin. Slower severing at lower

concentrations of ADF/Cofilin is consistent with concentration-dependent binding of ADF/Cofilin to filament sides; furthermore, a reduced plateau of cumulative severing events at higher concentrations of ADF/Cofilin is consistent with over-decoration

leading to filament stabilization [30,45,46]. Based on these observations, we used 150 nM (or lower) ADF/Cofilin in all remaining experiments, simplifying our severing analyses by minimizing the effects resulting from over-decoration.

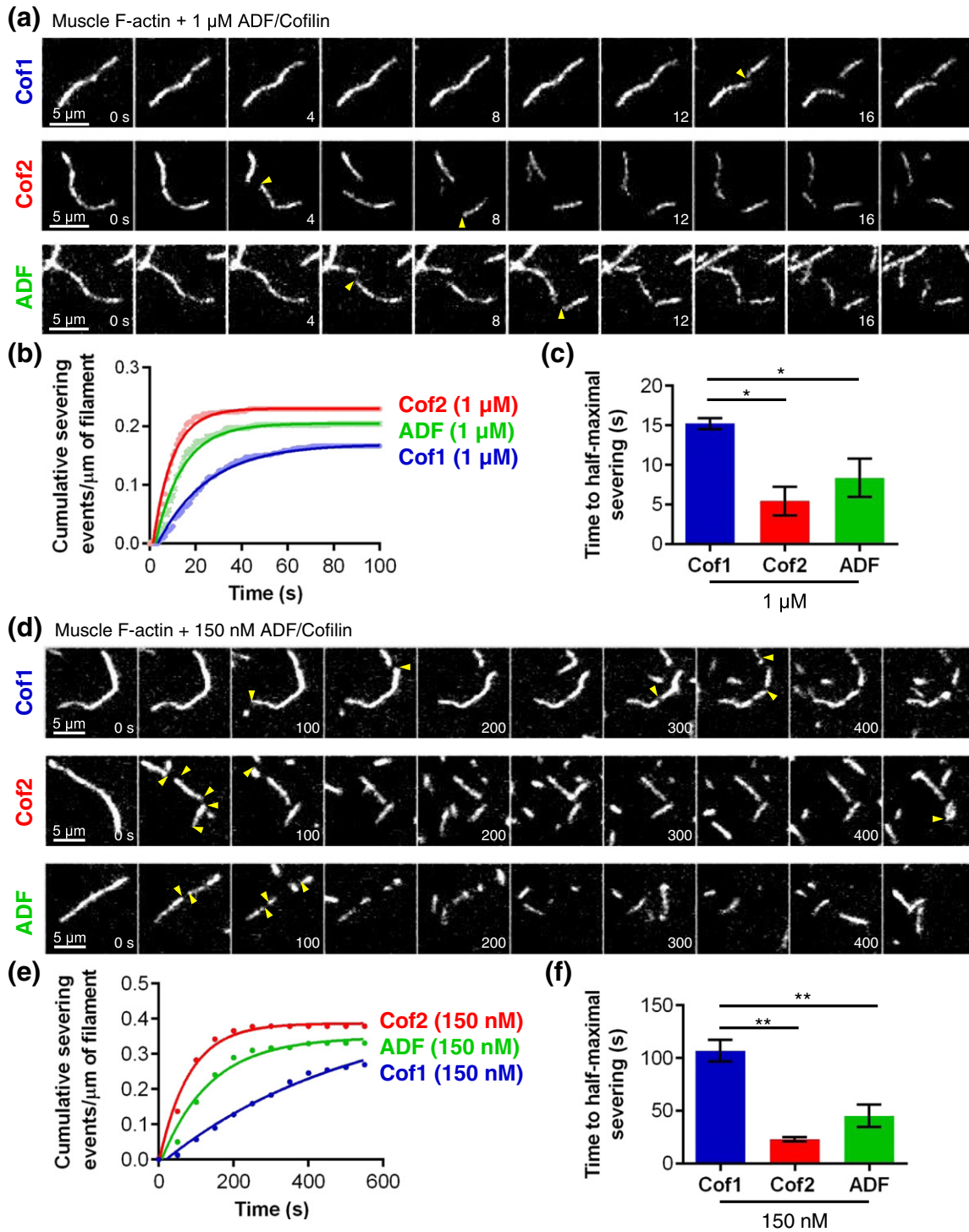
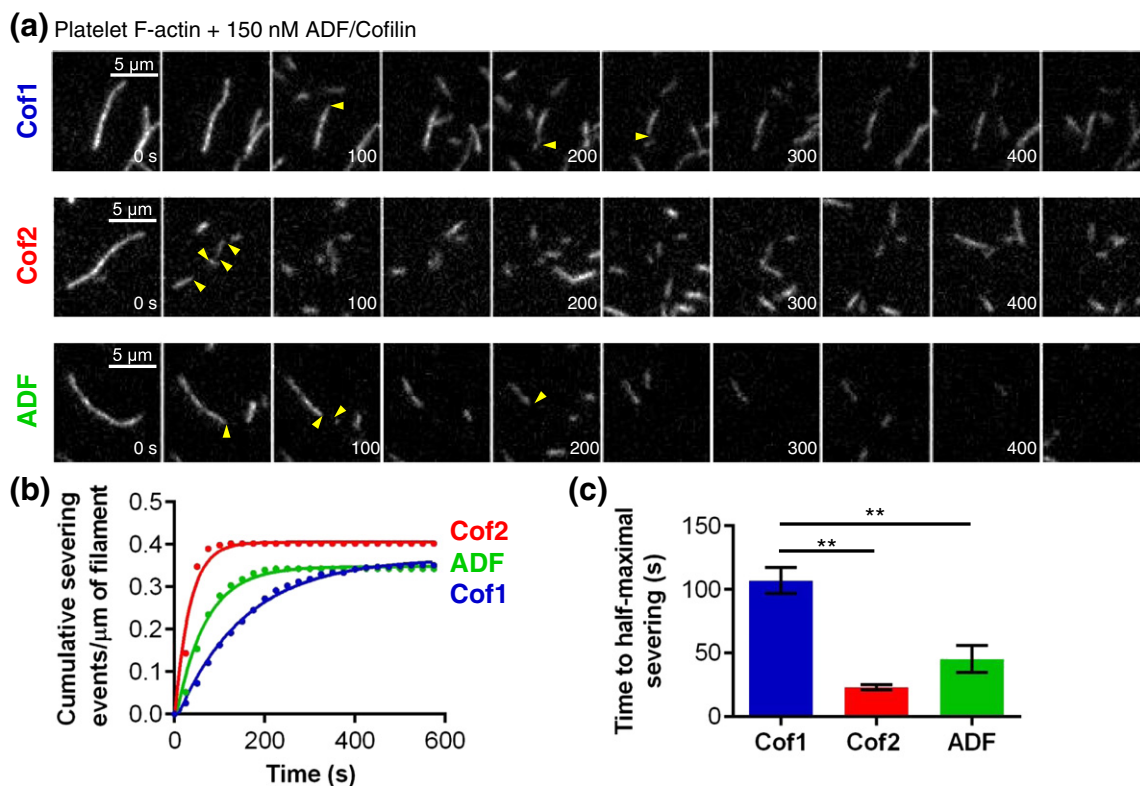


Fig. 2. (legend on next page)



**Fig. 3.** Rates of severing for 150 nM Cof1, Cof2, and ADF on filaments assembled from platelet actin. (a) Representative time-lapse images from TIRF microscopy experiments where OG-labeled actin filaments (platelet actin) were polymerized and tethered, and then 150 nM Cof1, Cof2, or ADF was flowed in. Severing events are indicated by yellow arrow heads. (b) Analysis of severing activities, in which each data point is the cumulative severing events per micron of filament at that time point, averaged from three independent experiments (20 filaments each). Data were fit to an exponential association curve. (c) Average time to half-maximal severing, calculated from exponential curve fits of data in (b). Error bars represent SEM. Statistical significance was determined using a one-way ANOVA analysis and Bonferroni multiple comparison test; \*\* indicates  $p < 0.05$ .

Because all of the assays above used rabbit muscle actin, we considered whether this might favor Cof2, the predominant isoform of ADF/Cofilin expressed in muscle tissue. Therefore, we additionally compared the severing activities of Cof1, Cof2, and ADF on filaments assembled from non-muscle (platelet) actin. Under these conditions, similar differences in severing activities were again observed (Fig. 3a–c; Movie S3), demonstrating that the higher severing efficiencies of Cof2 and ADF compared to Cof1 do not depend on the source of

actin. Muscle actin was used in all remaining experiments below.

### Cof2 and ADF each have stronger activity than Cof1 in promoting “enhanced severing” of either preformed or actively growing actin filaments

Recent studies have shown that mammalian Cof1 acts in concert with AIP1 and Coronin1B (Cor1B) to drive enhanced severing and pointed end disassembly of actin filaments *via* an ordered molecular

**Fig. 2.** Rates of actin filament severing by higher and lower concentrations of Cof1, Cof2, and ADF. (a) Representative time-lapse images from TIRF microscopy experiments where OG-labeled actin filaments were polymerized and tethered, and then 1  $\mu\text{M}$  Cof1, Cof2, or ADF was flowed in. Severing events are indicated by yellow arrow heads. (b) Analysis of severing activities, in which each data point is the cumulative severing events per micron of filament at that time point, averaged from three independent experiments (20 filaments each). Data were fit to an exponential association curve. (c) Average time to half-maximal severing, calculated from exponential curve fits of data in (b). Error bars represent SEM. Statistical significance was determined using a one-way ANOVA analysis and Bonferroni multiple comparison test; \* indicates  $p < 0.05$ . (d) Representative time-lapse images from TIRF microscopy experiments as in (a), except using 150 nM Cof1, Cof2, or ADF. (e) Analysis of severing activities as in (b), except that data were averaged from four independent experiments (20 filaments each). (f) Average time to half-maximal severing, calculated as in (c). \* indicates  $p < 0.05$ ; \*\* indicates  $p < 0.01$ .

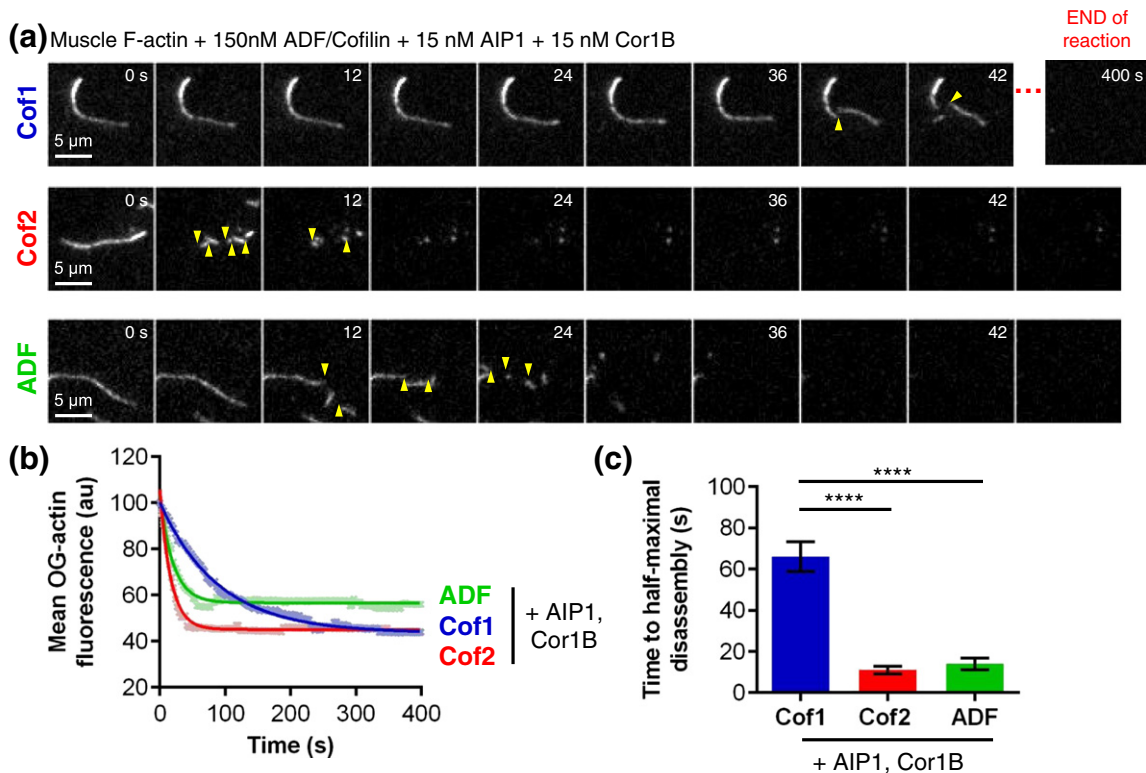


**Fig. 4.** Rates of enhanced actin filament disassembly by Cof1, Cof2, and ADF in the presence of co-factors Cor1B and AIP1. (a) Representative time-lapse images from TIRF microscopy experiments where OG-labeled actin filaments were polymerized and tethered, and then 15 nM Cor1B, 15 nM AIP1, and 150 nM of Cof1, Cof2, or ADF were flowed in. The last panel in the Cof1 montage was taken from the end of the reaction (400 s). Severing events are indicated by yellow arrow heads. (b) Average OG-actin fluorescence per field of view, averaged from four independent experiments and fit to an exponential decay curve. (c) Average time to half fluorescence decay based on exponential curve fits in (b). Error bars represent SEM. Statistical significance was determined using a one-way ANOVA analysis and Bonferroni or multiple comparison test; \*\*\*\* indicates  $p < 0.0001$ .

mechanism [24,47]. For this reason, we directly compared the abilities of human Cof1, Cof2, and ADF to promote enhanced actin disassembly in the presence of AIP1 and Cor1B. In these assays, we used 150 nM ADF/Cofilin, 15 nM Cor1B, and 15 nM AIP1, which approximates the molar ratio of these proteins found in cells [47–49]. For each of the three ADF/Cofilins, filament severing and disassembly was visibly faster in the presence of Cor1B and AIP1 (Fig. 4a and b; Movie S4) than in the absence (Fig. 2d). Filaments were rapidly severed into small fragments that were concurrently disassembled, which precluded accurate quantitation of severing. Therefore, we instead quantified loss of mean fluorescence (OG-actin) over time (Fig. 4b), which showed that Cof2 and ADF are sixfold and fivefold more efficient than Cof1 in disassembling actin in the presence of Cor1B and AIP1 (Fig. 4c). From these results, we conclude that all three human ADF/Cofilins productively function with AIP1 and Cor1B to induce enhanced actin disassembly. However, they

display different efficiencies in promoting enhanced disassembly, mirroring their differences in severing in the absence of the co-factors.

The experiments above were performed using preformed actin filaments, which consist primarily of ADP-actin subunits. To compare severing activities in a more physiological state, where filaments consist of subunits in different nucleotide states, we compared Cof1, Cof2, and ADF effects on dynamically growing filaments enriched in ADP +  $P_i$  subunits at their barbed ends. Filaments were polymerized by the combination of formins and profilin and simultaneously severed and disassembled along their lengths by the combined effects of ADF/Cofilin, AIP1, and Cor1B [24] (Fig. 5). The severing activities of Cof1, Cof2 and ADF were compared quantitatively by measuring the lengths of filament products in the reactions (Movie S5). ADF and Cof2 produced shorter filaments than Cof1, consistent with stronger severing activities (Fig. 5a and b). Cof2 also produced substantially shorter

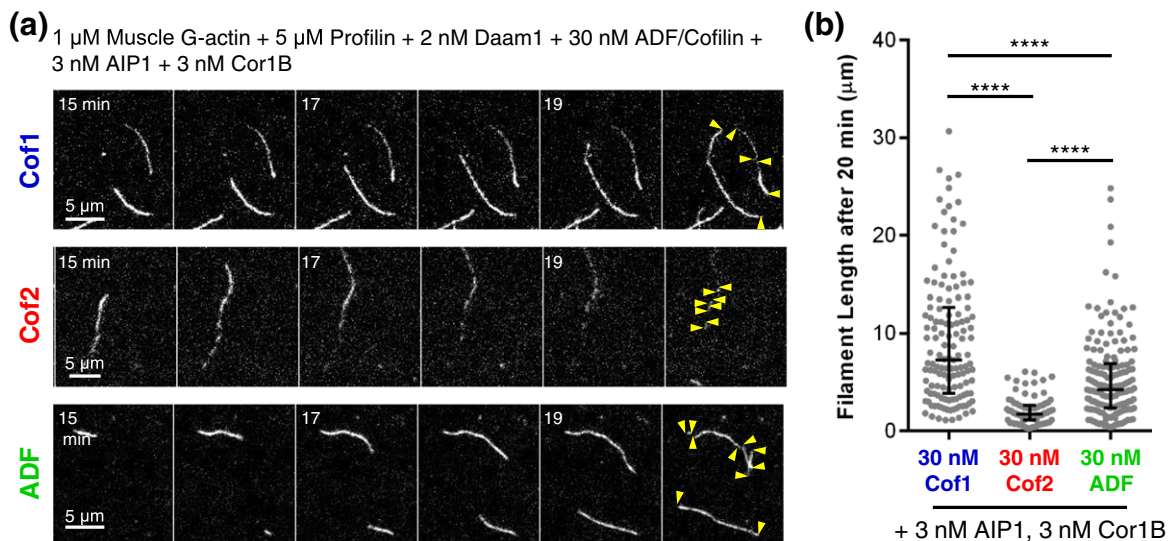


**Fig. 5.** Effects of Cof1, Cof2, and ADF on actively growing actin filaments in the presence of co-factors Cor1B and AIP1. (a) Representative time-lapse images from TIRF microscopy experiments using actively polymerizing labeled and tethered actin filaments. Reactions contain 1  $\mu$ M G-actin (10% OG-labeled, 0.5% biotinylated), 2 nM Daam1 (FH1-FH2-C), 5  $\mu$ M Profilin, 30 nM Cof1, Cof2, or ADF, 3 nM AIP1, and 3 nM Cor1B. Yellow arrows indicate filament ends 20 min after reaction initiation. (b) Distribution of filament lengths 20 min after reaction initiation. Median and interquartile range are shown. Statistical significance was determined using a Kruskal–Wallis and Dunn's multiple comparison test. \*\*\*\* indicates  $p < 0.0001$ .

filaments than ADF (Fig. 5b), suggesting that Cof2 may be particularly effective in severing dynamically growing filaments; this observations is in good agreement with a recent study showing that Cof2 (but not Cof1) severs BeF<sub>x</sub>-actin filaments, which mimic the ADP-P<sub>i</sub> state of F-actin [37].

#### Direct visualization of Cy3–Cof1 and Cy3–Cof2 during actin filament severing reveals mechanistic differences

To gain deeper insights into the differences in the severing efficiencies of the three ADF/Cofilins, we used multi-wavelength TIRF microscopy to directly compare their interactions on filaments during severing. In a previous study, we reengineered surface cysteine residues on human Cof1 to generate a Cy3-labeled Cof1 with severing activity indistinguishable from unlabeled wild-type human Cof1 [24]. To label Cof2, we applied a similar strategy, reengineering its surface cysteine residues (C39A and T63C substitutions) so that it could be labeled at a single site without interfering with function; Cy3–Cof2 showed severing activity indistinguishable from unlabeled Cof2 (Fig. 6a). However, we were unable to produce functionally labeled human ADF by this strategy because it has eight surface cysteine residues, many of which are near key actin binding surfaces. For this reason, we

focused our analysis on comparing Cy3–Cof1 and Cy3–Cof2 interactions with actin filaments.

Multi-wavelength TIRF microscopy analysis showed that Cy3–Cof1 and Cy3–Cof2 each first appear on filaments as faint spots that steadily intensify over time (Fig. 6b; Movie S6). These observations suggest a cooperative binding mechanism, as previously reported for yeast Cofilin and human Cof1 [22–24,27]. Cy3–Cof1 and Cy3–Cof2 also accumulated on filaments with similar kinetics preceding severing, as assessed by two different measurements. First, Cy3–Cof1 and Cy3–Cof2 showed similar kinetics of total fluorescence accumulation along filaments (Fig. 6c). Second, they showed similar rates of fluorescence accumulation in the individual patches on filaments (Fig. 6d). These data are in good agreement with our pyrene-quenching data, which indicate that Cof1, Cof2, and ADF bind F-actin with similar affinities (Fig. 1d–f). Further analysis of the data also revealed a substantially longer time interval between first appearance of Cofilin on the filament and severing at that location for Cy3–Cof1 compared to Cy3–Cof2 (median = 78 s and 28 s, respectively; examples in Fig. 6e; quantified in Fig. 6f). Consistent with these measurements, Cy3–Cof1 patches also showed increased levels of fluorescence intensity by 1 s prior to severing compared to Cy3–Cof2 patches (Fig. 6g). Thus, Cy3–Cof1 and Cy3–Cof2 bind to filaments with similar kinetics and affinities, yet Cof2 induces much more

rapid severing. Finally, our analysis showed that severing events occurred preferentially on the pointed end side of where Cof1 or Cof2 bind, resulting in Cy3–Cof1 and Cy3–Cof2 preferentially decorating the newly generated pointed end after severing (Fig. 6h), consistent with another recent study [28].

### Discussion

In this study, we have performed what is to our knowledge the first real-time TIRF microscopy analysis comparing the severing efficiencies of the three mammalian ADF/Cofilin proteins: Cof1, Cof2,

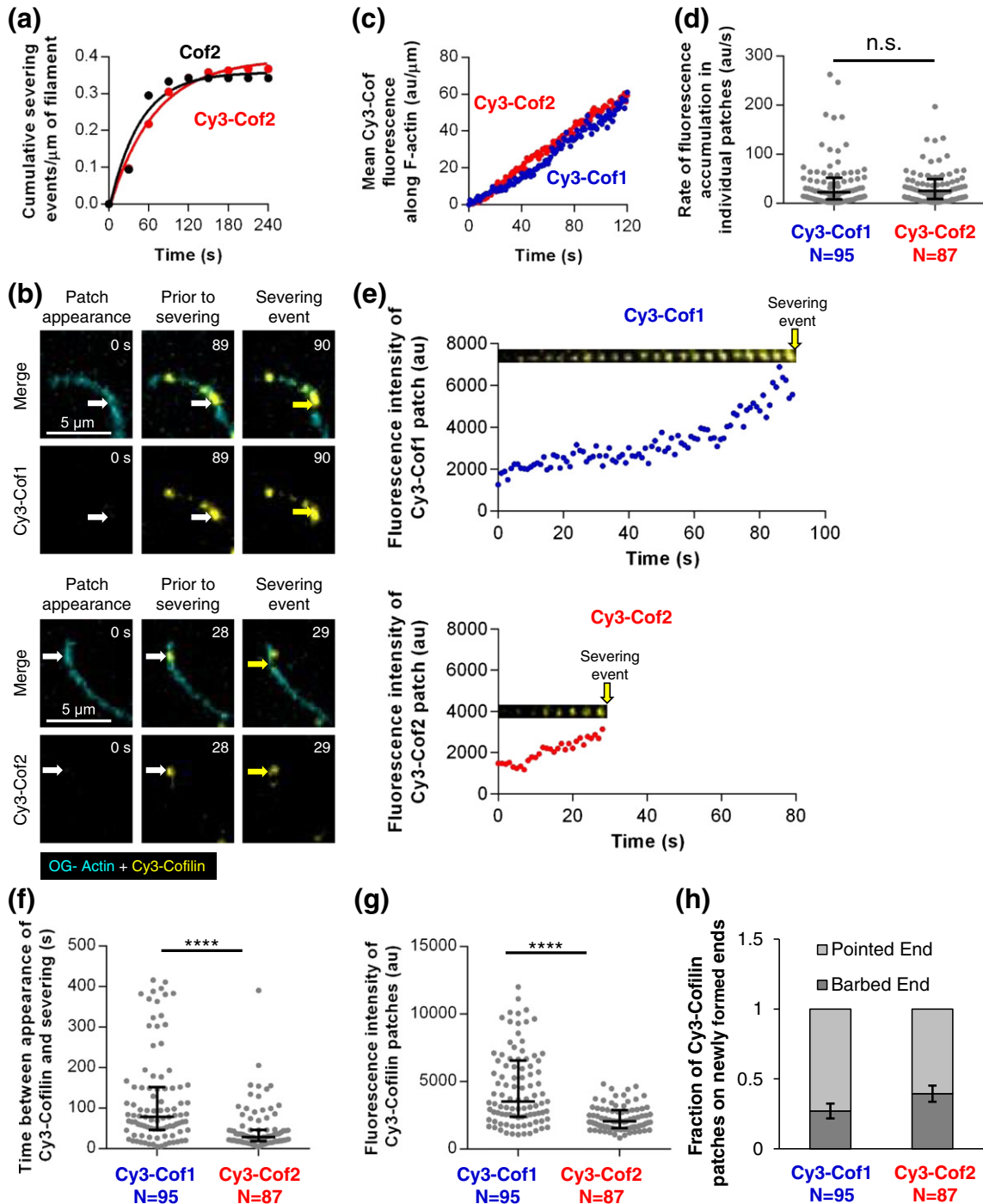


Fig. 6. (legend on next page)

and ADF. Initially, we used tethered preformed filaments in the absence of free actin monomers, so that severing effects could be quantified independent of possible indirect effects resulting from ADF/Cofilin competition between filaments and monomers (Figs. 2-4). However, similar differences were again observed when we compared Cof1, Cof2, and ADF severing effects on dynamically growing actin filaments (Fig. 5). Under both conditions, Cof2 and ADF had substantially stronger severing activities compared to Cof1 (Figs. 2-5). In addition, we observed these severing differences at lower and higher concentrations of ADF/Cofilin (Fig. 2), and using either muscle or non-muscle actin (Figs. 2 and 3), and in the presence of actin disassembly co-factors Cor1B and AIP1 (Figs. 4 and 5). Thus, under multiple conditions, the severing activity differences were observed. It is possible that Cof1, Cof2, and ADF also have differences in promoting subunit dissociation from filament ends, but this was not possible to measure in this experimental system because the severed fragments diffuse out of the field of view before changes in filament length could be observed.

Our results using direct visualization in real time by TIRF microscopy agree well with previous studies using other techniques, which suggested that ADF is stronger than Cof1 in severing and disassembling actin filaments [36]. On the other hand, they differ from other studies suggesting that Cof2 has weaker severing activity than Cof1 [9]. More specifically, these previous studies compared the following: (i) the effects of Cof1 and ADF on severing using visual assays (fluorescence and electron microscopy) at fixed time points [9,36], (ii) the effects of Cof1 and Cof2 on F-actin disassembly using bulk assays [37], and (iii) the effects of Cof1, Cof2, and ADF on

disassembly using F-actin sedimentation assays [9]. As mentioned earlier (see Introduction), these studies led to different conclusions about the relative efficiencies of Cof1, Cof2, and ADF in severing and disassembling filaments. Our study provides new insights into this question, because we directly visualized and quantified severing events in real time at the single filament level. We show that Cof2 and ADF sever actin filaments more efficiently than Cof1 in assays either using preformed filaments, which lack actin monomers, or assays containing actively growing filaments, which contain 1  $\mu$ M Profilin-bound actin monomers. This is not necessarily inconsistent with previous reports showing that Cof2 has reduced severing activity in the presence of actin monomers, since Profilin was not present [9].

To gain mechanistic insights into the differences in severing efficiency for the three ADF/Cofilins, we generated fluorescently labeled Cof1 and Cof2, which we used to directly visualize the proteins on actin filaments during severing. Surface cysteines were reengineered to allow direct dye labeling at a single residue without altering the activity of the protein. Furthermore, Cof1 and Cof2 were labeled with the same fluorophore (Cy3) to the same degree, and studied in parallel by multi-wavelength TIRF microscopy using identical settings, enabling a direct comparison. As mentioned above, ADF posed significant challenges to labeling, as it has eight surface-exposed cysteine residues. Therefore, we focused on comparing Cof1 and Cof2. Cy3-Cof1 and Cy3-Cof2 each bound to filaments with similar kinetics, appearing initially as faint patches that intensified over time at a similar rate (Fig. 6b-d). Thus, human Cof2 binds cooperatively to filaments, similar to human Cof1 and yeast Cof1 [22-24]. Furthermore, these kinetic data agree with our observation that Cof1,

**Fig. 6.** Multi-wavelength TIRF microscopy analysis of Cy3-Cof1 and Cy3-Cof2 interacting with filaments during severing. (a) Cy3-Cof2 and unlabeled Cof2 (200 nM each) have similar actin filament severing activities. Each data point represents the cumulative severing events per micron of filament at that time point, averaged from 20 filaments. Data were fit to an exponential association curve. (b) Representative time-lapse images from multi-wavelength TIRF microscopy experiments in which OG-labeled actin filaments were first polymerized and tethered, and then 150 nM Cy3-Cof1 or Cy3-Cof2 were flowed in. The first panel ("patch appearance") represents the first time point at which association of Cy3-Cofilin in a spot on the filament could be detected (indicated by white arrow). The middle panel shows the same Cy3-Cofilin spot 1 s before severing. The third panel shows the severing event (indicated by the yellow arrow). (c) Kinetics of Cy3-Cof1 and Cy3-Cof2 association with filaments prior to severing. Each data point is the average Cy3 fluorescence accumulation on filaments at that time point, averaged from three independent experiments (20 filaments each). (d) Distribution of rates of Cy3-Cof1 or Cy3-Cof2 fluorescence accumulation in individual patches on actin filaments, analyzed from movies as in (B). Median and interquartile range are shown. (e) Graphs show fluorescence intensity of Cy3-Cofilin patches in (b) over time, from the point of initial patch appearance until severing. The montages above each graph follow the same time scale (x-axis) and are time-lapse images (every 4 s) of representative Cy3-Cofilin patches from movies in (b). Yellow arrow indicates severing event. (f) Distribution of time intervals between first detection of Cy3-Cof1 or Cy3-Cof2 patches on actin filaments and a severing event at the same location. Median and interquartile range are shown. (g) Distribution of fluorescence intensities of Cy3-Cof1 and Cy3-Cof2 patches on filaments 1 s before severing. Median and interquartile range are shown. (h) Fraction of filament severing events resulting in a Cy3-Cof1 or Cy3-Cof2 patch remaining at the newly formed barbed versus pointed end. Statistical significance was determined using Mann-Whitney two-sample *t* tests; n.s. indicates  $p > 0.5$ , \*\*\*\* indicates  $p < 0.0001$ . Error bars are binomial distribution errors.

Cof2, and ADF bind to F-actin with similar affinities in pyrene-quenching assays (Fig. 1d–f).

Further analysis of our multi-wavelength TIRF data revealed that severing occurred at sites with significantly lower levels of decoration by Cof2 compared to Cof1 (Fig. 6g). This was also reflected in Cy3–Cof2 showing a reduced time interval from initial binding on filaments to severing (Fig. 6f). Although our results do not explain how the same levels of Cof2 decoration induce more rapid severing compared to Cof1, they raise intriguing possibilities. For instance, the longer time interval for Cof1 between first appearance on a filament and severing at the same site could reflect a requirement for higher levels of Cof1 (compared to Cof2) to induce severing, or instead a delayed conformational response to Cof1 binding. Another possibility, not mutually exclusive from those above, is that Cof2 establishes unique contacts with F-actin and/or triggers distinct conformational changes in F-actin to induce fragmentation more efficiently. It is also interesting to consider how sequence differences between Cof1, Cof2, and ADF account for the differences in their severing activities. Previous studies found that differences in the actin-binding residues of the three ADF/Cofilins map to the F-site [9], and a recent study on yeast Cof1 demonstrated that point mutations in its F-site drastically enhance severing activity [50].

How might differences in Cof1, Cof2, and ADF severing activities be coupled to their distinct physiological functions? Most non-muscle cell and tissue types express both Cof1 and ADF, typically at distinct levels, and some express all three ADF/Cofilins, including neurons, oligodendrocytes, and keratinocytes [9,12,13]. Furthermore, cardiac muscle cells express both Cof1 and Cof2 [37]. In light of our results, it is tempting to speculate that cells may express different levels and ratios of the three ADF/Cofilins in order to tune rates of actin network turnover. Another possibility, not mutually exclusive from the first, is that cells express multiple ADF/Cofilins in order to position them downstream of different signaling pathways and thus gain more regulatory control over actin turnover. Cof1, Cof2, and ADF appear to be regulated similarly by phosphorylation-dephosphorylation of Ser<sup>3</sup> through LIM kinase and Slingshot phosphatase, respectively, and by sequestration and release at the plasma membrane by PIP<sub>2</sub> and PLC $\gamma$ -mediated PIP<sub>2</sub>-hydrolysis, respectively [51–53]. However, a new form of regulation by cysteine oxidation has been demonstrated for Cof1, and it is not yet clear whether ADF and Cof2 are regulated by this mechanism [54]. Finally, an important question to address will be whether different ADF/Cofilins have specialized roles in disassembling actin filament networks depending on how they are decorated by other actin binding proteins such as tropomyosins and/or spatially organized, for example, linear versus branched, loose versus tightly cross-

linked, and parallel versus antiparallel. It is our hope that the discoveries made here help inspire new investigation into the emerging functional diversity in the ADF/Cofilin family.

## Experimental Procedures

### Plasmids and protein purification

Plasmids for expressing human Cof1, Cof2, and ADF were generously provided by Dr. David Kovar (University of Chicago). To generate fluorescently labeled Cof1, we used a reengineered Cof1 construct that we recently demonstrated is fully functional [24]. For labeling Cof2, we applied a similar strategy, in this case using site-directed mutagenesis to introduce C39A mutation, then introducing a T63C mutation, such that Cof2 has one surface Cys residue (Cys<sup>63</sup>) for labeling at a site that does not interfere with its activities (Fig. 6a). All constructs were verified by DNA sequencing. Rabbit skeletal muscle actin was purified as described [55]. Human platelet actin was purchased from Cytoskeleton Inc. (Denver, CO). Fluorescent rabbit muscle actin, labeled on Cys<sup>374</sup> with OG maleimide (Life Technologies; Carlsbad, CA) was generated as described [56]. Cor1B and AIP1 were expressed in HEK393T cells and purified as previously described [24]. The formin Daam1 (6his-FH1-FH2-C) was expressed in yeast and purified by sequential Ni<sub>2</sub>-NTA and gel filtration chromatography as described [57]. Human profilin was expressed and purified from *Escherichia coli* as described [58].

Human Cof1, Cof2, and ADF were expressed in BL21 (DE3) *E. coli* by growing cells to log phase at 37 °C in TB medium, then inducing expression using 1 mM isopropyl beta-D-1-thiogalactopyranoside at 18 °C for 16 h. Cells were harvested by centrifugation and pellets were stored at –80 °C. Frozen pellets were resuspended in 20 mM Tris (pH 8.0), 50 mM NaCl, 1 mM DTT, and protease inhibitors. Cells were lysed by sonication, and the lysate was cleared by centrifugation at 30,000g for 30 min in a Fiberlite F13-14X50CY rotor (Thermo Scientific, Waltham, MA). The lysate was loaded on a 5 ml HiTrap HP Q column (GE Healthcare Biosciences, Pittsburgh, PA), and the flow-through was harvested and dialyzed against 20 mM Hepes (pH 6.8), 25 mM NaCl, and 1 mM DTT. Dialyzed proteins were then fractionated on a 5 ml HiTrap SP FF column (GE Healthcare Biosciences), eluted using a linear gradient of NaCl (20–500 mM). Fractions containing ADF/Cofilin were concentrated, dialyzed into 20 mM Tris (pH 8.0), 50 mM KCl, and 1 mM DTT, aliquoted and stored at –80 °C.

For generating fluorescently labeled Cof1 and Cof2, the proteins were purified as above, except eluted from the HiTrap SP FF column with PBS, reduced in 0.3 mM TCEP for 30 min on ice, and then incubated overnight at 4 °C with a threefold molar excess of Cy3-maleimide (GE Healthcare Biosciences). Excess dye was quenched using 5 mM DTT and removed by passing the labeled proteins over a PD-10 column equilibrated in 20 mM Tris (pH 8.0), 50 mM KCl, and 1 mM DTT. Final labeling efficiencies (82% for Cy3–Cof1, 54% for Cy3–Cof2) were determined spectrophotometrically using the absorbance (at 550 nm) and extinction coefficient (150,000 M<sup>-1</sup> cm<sup>-1</sup>) for Cy3,

combined with the absorbance (at 280 nm) and estimated extinction coefficient ( $14,440 \text{ M}^{-1} \text{ cm}^{-1}$  for Cof1,  $18,450 \text{ M}^{-1} \text{ cm}^{-1}$  for Cof2). The absorption at 280 nm was corrected for background fluorescence from the dye (correction factor 0.024). Importantly, Cy3–Cof1 and Cy3–Cof2 were diluted with unlabeled protein to the same labeling percentage for all direct comparisons (Fig. 6b–h).

### G-actin nucleotide exchange assays

Nucleotide exchange rates on ADP-G-actin were determined by measuring the increase in fluorescence upon incorporation of  $\epsilon$ -ATP (Sigma-Aldrich, St. Louis, MO). To prepare ADP-G-actin,  $2 \mu\text{M}$  rabbit muscle actin was treated with analytical grade anion exchange resin (BioRad, Los Angeles, CA) and incubated with hexokinase (Sigma-Aldrich) and excess ADP overnight at  $4^\circ\text{C}$ . Next,  $2 \mu\text{M}$  of ADP-G-actin was mixed with the indicated concentration of ADF/Cofilin in CDT buffer [ $0.2 \text{ mM CaCl}_2$ ,  $0.2 \text{ mM DTT}$ ,  $10 \text{ mM Tris}$  (pH 8.0)] or buffer alone and added to  $50 \mu\text{M}$   $\epsilon$ -ATP. The reaction was monitored for 200 s at 350-nm excitation and 410-nm emission at  $25^\circ\text{C}$  in a fluorescence spectrophotometer (Photon Technology International, Lawrenceville, NJ). Exchange rates were calculated by linear fitting of the first 50 s of each reaction curve. Prism 5.0 was used to fit the resulting data to a hyperbolic function of the following form  $f = y_0 - ax/(b + x)$ , where the variable  $b$  is the apparent  $K_{\text{app}}$ .

### F-actin binding assays

Rabbit muscle actin (10% pyrene labeled) was polymerized in F-Buffer [ $20 \text{ mM Tris}$  (pH 7.5),  $50 \text{ mM KCl}$ ,  $0.2 \text{ mM ATP}$ ,  $1 \text{ mM MgCl}_2$ , and  $1 \text{ mM DTT}$ ]. To allow binding to reach equilibrium,  $2 \mu\text{M}$  F-actin was mixed with different concentrations of Cof1, Cof2, or ADF, and incubated overnight at  $25^\circ\text{C}$ . Pyrene-F-actin fluorescence was measured in a plate reader (Infinite M200; Tecan, Männedorf, Switzerland) at excitation and emission wavelengths of 365 and 407 nm at  $25^\circ\text{C}$ . Binding curves were fit to a cooperative function of the form  $f = (B_{\text{max}} * x^n)/(K_d^n + x^n)$  to determine the  $K_d$ . To verify that loss of fluorescence was due to F-actin binding rather than depolymerization, reactions were centrifuged at 90,000 rpm for 30 min in a TLA120 instrument (Beckman Instruments, Brea, CA), and actin levels in the pellet were analyzed on Coomassie-stained gels.

### TIRF microscopy

For all experiments,  $24 \times 60 \text{ mm}$  coverslips (Fisher Scientific, Pittsburg, PA) were cleaned by successive sonications as follows: 60 min in detergent, 20 min in  $1 \text{ M KOH}$ , 20 min in  $1 \text{ M HCl}$  min, and 60 min in ethanol. Coverslips were then washed extensively with  $\text{ddH}_2\text{O}$  and dried in an  $\text{N}_2$ -stream. A solution of 80% ethanol (pH 2.0),  $2 \text{ mg/ml}$  methoxy-poly (ethylene glycol)-silane, and  $2 \mu\text{g/ml}$  biotin-poly (ethylene glycol)-silane (Laysan Bio Inc., Arab, AL) was prepared and layered on the clean coverslip ( $200 \mu\text{l}$  per slide). The coverslips incubated for 16 h at  $70^\circ\text{C}$ . To assemble flow cells, PEG-coated coverslips were rinsed extensively with  $\text{ddH}_2\text{O}$  and dried in an  $\text{N}_2$ -stream, then attached to a prepared flow chamber

(Ibidi; Martinsried, German) with double sided tape ( $2.5 \text{ cm} \times 2 \text{ mm} \times 120 \mu\text{m}$ ) and 5-min epoxy resin. Flow cells were prepared immediately before use by sequential incubations as follows: 3 min in HEK-BSA [ $20 \text{ mM Hepes}$  (pH 7.5),  $1 \text{ mM EDTA}$ ,  $50 \text{ mM KCl}$ ,  $1\% \text{ BSA}$ ], 30 s in streptavidin ( $0.1 \text{ mg/ml}$  in PBS), a fast rinse in HEK-BSA, and then equilibration in  $1 \times \text{TIRF buffer}$  [ $10 \text{ mM imidazole}$ ,  $50 \text{ mM KCl}$ ,  $1 \text{ mM MgCl}_2$ ,  $1 \text{ mM EGTA}$ ,  $0.2 \text{ mM ATP}$ ,  $10 \text{ mM DTT}$ ,  $15 \text{ mM glucose}$ ,  $20 \mu\text{g/ml}$  catalase,  $100 \mu\text{g/ml}$  glucose oxidase, and  $0.5\% \text{ methylcellulose}$  ( $4000 \text{ cP}$ ; pH 7.5)]. To initiate reactions, actin monomers ( $10\% \text{ OG-labeled}$ ,  $0.5\% \text{ biotinylated}$ ) were diluted to  $1 \mu\text{M}$  in TIRF buffer and immediately transferred to a flow chamber. To measure severing/disassembly, actin was polymerized at room temperature until filaments reached lengths of approximately  $10\text{--}15 \mu\text{m}$ , then free actin monomers were washed out, and proteins of interest in TIRF buffer were introduced by flow-in. For treadmill assays (Fig. 5), proteins of interest were mixed with  $1 \mu\text{M}$  actin monomers ( $10\% \text{ OG-labeled}$  actin;  $0.5\% \text{ biotin-actin}$ ), then immediately transferred to a flow chamber for imaging. Time-lapse TIRF microscopy was performed using a Nikon-Ti200 inverted microscope equipped with a  $150 \text{ mW Ar-Laser}$  (Mellot Griot, Carlsbad, CA), a TIRF-objective with an N.A. of 1.49 (Nikon Instruments Inc., New York, NY), and an EMCCD camera (Andor Ixon, Belfast, Northern Ireland). During recordings, optimal focus was maintained using the perfect focus system (Nikon Instruments Inc). The pixel size corresponded to  $0.27 \mu\text{m}$ .

TIRF data were analyzed using ImageJ software (NIH, Bethesda, MD). Before each analysis, the background was subtracted using the background subtraction tool (rolling ball radius 50 pixels). Filament severing rates were calculated by measuring the initial lengths of filaments before flow-in, then scoring severing events after flow-in of proteins of interest. Prism 5.0 was used for exponential curve fitting to determine the time to half-maximal cumulative severing events and for statistical analysis. In treadmill assays (Fig. 5), actin filament lengths were measured 20 min after reaction initiation, and only filaments nucleated during the first 18 min were analyzed. For kinetic analysis of Cy3–Cof1 and Cy3–Cof2 binding to filaments, OG-actin filaments were traced based on the signal in the 488-nm channel and saved as a region of interest, and then used to determine the fluorescence profiles in the 561-nm channel using the Plot Z-axis profile tool. For analysis of Cy3–Cof1 and Cy3–Cof2 patches, severing events were scored, and then a  $1 \mu\text{m} \times 1 \mu\text{m}$  box was drawn around the Cy3–Cofilin patch one frame prior to severing, and saved as a region of interest. The fluorescence intensity of the Cy3 fluorescence in the boxes was determined using the Measure Integrated Density function.

Supplementary data to this article can be found online at <http://dx.doi.org/10.1016/j.jmb.2016.03.006>.

### Acknowledgments

We are grateful to James Bamberg, Sean Guo, Richa Jaiswal, and Adam Johnston for helpful discussions and/or comments on the manuscript, and to Julian Eskin for generating the graphical

abstract. This work was supported by a summer undergraduate fellowship to S.C. awarded by Brandeis University, by a grant from the National Science Foundation (DMR-MRSEC-0820429) to Brandeis, and by a grant from the NIH (R01 GM063691) to B.L.G.

Received 9 December 2015;

Received in revised form 29 February 2016;

Accepted 9 March 2016

Available online 17 March 2016

**Keywords:**

Cofilin;  
ADF;  
Coronin;  
AIP1;  
actin disassembly

**Abbreviations used:**

ADF, actin-depolymerizing factor; Cof1, Cofilin-1; Cof2, Cofilin-2; Srv2/CAP, suppressor of Ras<sup>Val2</sup>/cyclase-associated protein; AIP1, actin-interacting protein 1; Cor1B, Coronin1B; TIRF, total internal reflection fluorescence.

## References

- [1] J.R. Bamburg, A. McGough, S. Ono, Putting a new twist on actin: ADF/cofilins modulate actin dynamics, *Trends Cell Biol.* 9 (1999) 364–370.
- [2] B.W. Bernstein, J.R. Bamburg, ADF/cofilin: a functional node in cell biology, *Trends Cell Biol.* 20 (2010) 187–195.
- [3] S. Ono, Mechanism of depolymerization and severing of actin filaments and its significance in cytoskeletal dynamics, *Int. Rev. Cytol.* 258 (2007) 1–82.
- [4] M. Poukkula, E. Kremneva, M. Serlachius, P. Lappalainen, Actin-depolymerizing factor homology domain: a conserved fold performing diverse roles in cytoskeletal dynamics, *Cytoskeleton (Hoboken)* 68 (2011) 471–490.
- [5] A.L. Moon, P.A. Janmey, K.A. Louie, D.G. Drubin, Cofilin is an essential component of the yeast cortical cytoskeleton, *J. Cell Biol.* 120 (1993) 421–435.
- [6] K. Iida, K. Moriyama, S. Matsumoto, H. Kawasaki, E. Nishida, I. Yahara, Isolation of a yeast essential gene, COF1, that encodes a homologue of mammalian cofilin, a low-M(r) actin-binding and depolymerizing protein, *Gene* 124 (1993) 115–120.
- [7] K.C. Gunsalus, S. Bonaccorsi, E. Williams, F. Verni, M. Gatti, M.L. Goldberg, Mutations in *twinstar*, a *Drosophila* gene encoding a cofilin/ADF homologue, result in defects in centrosome migration and cytokinesis, *J. Cell Biol.* 131 (1995) 1243–1259.
- [8] H. Aizawa, K. Sutoh, S. Tsubuki, S. Kawashima, A. Ishii, I. Yahara, Identification, characterization, and intracellular distribution of cofilin in *Dictyostelium discoideum*, *J. Biol. Chem.* 270 (1995) 10923–10932.
- [9] M.K. Vartiainen, T. Mustonen, P.K. Mattila, P.J. Ojala, I. Thesleff, J. Partanen, et al., The three mouse actin-depolymerizing factor/cofilins evolved to fulfill cell-type-specific requirements for actin dynamics, *Mol. Biol. Cell* 13 (2002) 183–194.
- [10] P. Hotulainen, E. Paunola, M.K. Vartiainen, P. Lappalainen, Actin-depolymerizing factor and cofilin-1 play overlapping roles in promoting rapid F-actin depolymerization in mammalian nonmuscle cells, *Mol. Biol. Cell* 16 (2005) 649–664.
- [11] L.H. Tahtamouni, A.E. Shaw, M.H. Hasan, S.R. Yasin, J.R. Bamburg, Non-overlapping activities of ADF and cofilin-1 during the migration of metastatic breast tumor cells, *BMC Cell Biol.* 14 (2013) 45.
- [12] G. Kanellos, J. Zhou, H. Patel, R.A. Ridgway, D. Huels, C.B. Gurniak, E. Sandilands, N.O. Carragher, O.J. Sansom, W. Witke, V.G. Brunton, M.C. Frame, ADF and cofilin1 control actin stress fibers, nuclear integrity, and cell survival, *Cell Rep.* 13 (2015) 1949–1964.
- [13] J.B. Zuchero, M.M. Fu, S.A. Sloan, A. Ibrahim, A. Olson, A. Zaremba, et al., CNS myelin wrapping is driven by actin disassembly, *Dev. Cell* 34 (2015) 152–167.
- [14] C.B. Gurniak, E. Perlas, W. Witke, The actin depolymerizing factor n-cofilin is essential for neural tube morphogenesis and neural crest cell migration, *Dev. Biol.* 278 (2005) 231–241.
- [15] S. Ikeda, L.A. Cunningham, D. Boggess, N. Hawes, C.D. Hobson, J.P. Sundberg, et al., Aberrant actin cytoskeleton leads to accelerated proliferation of corneal epithelial cells in mice deficient for destrin (actin depolymerizing factor), *Hum. Mol. Genet.* 12 (2003) 1029–1037.
- [16] P.B. Agrawal, M. Joshi, T. Savic, Z. Chen, A.H. Beggs, Normal myofibrillar development followed by progressive sarcomeric disruption with actin accumulations in a mouse Cfl2 knockout demonstrates requirement of cofilin-2 for muscle maintenance, *Hum. Mol. Genet.* 21 (2012) 2341–2356.
- [17] Y. Estornes, F. Gay, J.C. Gevrey, S. Navoizat, M. Nejari, J.Y. Scoazec, et al., Differential involvement of destrin and cofilin-1 in the control of invasive properties of Lsreco1 human colon cancer cells, *Int. J. Cancer* 121 (2007) 2162–2171.
- [18] K.C. Flynn, F. Hellal, D. Neukirchen, S. Jacob, S. Tahirovic, S. Dupraz, et al., ADF/cofilin-mediated actin retrograde flow directs neurite formation in the developing brain, *Neuron* 76 (2012) 1091–1107.
- [19] G. Hild, L. Kalmar, R. Kardos, M. Nyitrai, B. Bugyi, The other side of the coin: functional and structural versatility of ADF/cofilins, *Eur. J. Cell Biol.* 93 (2014) 238–251.
- [20] W.A. Elam, H. Kang, E.M. De la Cruz, Biophysics of actin filament severing by cofilin, *FEBS Lett.* 587 (2013) 1215–1219.
- [21] A. McGough, B. Pope, W. Chiu, A. Weeds, Cofilin changes the twist of F-actin: implications for actin filament dynamics and cellular function, *J. Cell Biol.* 138 (1997) 771–781.
- [22] C. Suarez, J. Roland, R. Boujemaa-Paterski, H. Kang, B.R. McCullough, A.C. Reymann, et al., Cofilin tunes the nucleotide state of actin filaments and severs at bare and decorated segment boundaries, *Curr. Biol.* 21 (2011) 862–868.
- [23] F. Chaudhry, D. Breitsprecher, K. Little, G. Sharov, O. Sokolova, B.L. Goode, Srv2/cyclase-associated protein forms hexameric shurikens that directly catalyze actin filament severing by cofilin, *Mol. Biol. Cell* 24 (2013) 31–41.
- [24] S. Jansen, A. Collins, S.M. Chin, C.A. Ydenberg, J. Gelles, B.L. Goode, Single-molecule imaging of a three-component ordered actin disassembly mechanism, *Nat. Commun.* 6 (2015) 7202.
- [25] A.A. Bobkov, A. Muhlrad, K. Kokabi, S. Vorobiev, S.C. Almo, E. Reisler, Structural effects of cofilin on longitudinal contacts in F-actin, *J. Mol. Biol.* 323 (2002) 739–750.

- [26] V.E. Galkin, A. Orlova, D.S. Kudryashov, A. Solodukhin, E. Reisler, G.F. Schroder, et al., Remodeling of actin filaments by ADF/cofilin proteins, *Proc. Natl. Acad. Sci. U. S. A.* 108 (2011) 20568–20572.
- [27] H. Kang, M.J. Bradley, W. Cao, K. Zhou, E.E. Grintsevich, A. Michelot, et al., Site-specific cation release drives actin filament severing by vertebrate cofilin, *Proc. Natl. Acad. Sci. U. S. A.* 111 (2014) 17821–17826.
- [28] K.X. Ngo, N. Kodera, E. Katayama, T. Ando, T.Q. Uyeda, Cofilin-induced unidirectional cooperative conformational changes in actin filaments revealed by high-speed atomic force microscopy, *Elife* 4 (2015).
- [29] B.R. McCullough, L. Blanchoin, J.L. Martiel, E.M. De la Cruz, Cofilin increases the bending flexibility of actin filaments: implications for severing and cell mechanics, *J. Mol. Biol.* 381 (2008) 550–558.
- [30] E. Andrianantoandro, T.D. Pollard, Mechanism of actin filament turnover by severing and nucleation at different concentrations of ADF/cofilin, *Mol. Cell* 24 (2006) 13–23.
- [31] M.A. Mikati, D. Breitsprecher, S. Jansen, E. Reisler, B.L. Goode, Coronin enhances actin filament severing by recruiting cofilin to filament sides and altering F-actin conformation, *J. Mol. Biol.* 427 (2015) 3137–3147.
- [32] K.P. Normoyle, W.M. Brieher, Cyclase-associated protein (CAP) acts directly on F-actin to accelerate cofilin-mediated actin severing across the range of physiological pH, *J. Biol. Chem.* 287 (2012) 35722–35732.
- [33] A.V. Nadkarni, W.M. Brieher, Aip1 destabilizes cofilin-saturated actin filaments by severing and accelerating monomer dissociation from ends, *Curr. Biol.* 24 (2014) 2749–2757.
- [34] Q. Chen, N. Courtemanche, T.D. Pollard, Aip1 promotes actin filament severing by cofilin and regulates constriction of the cytokinetic contractile ring, *J. Biol. Chem.* 290 (2015) 2289–2300.
- [35] L. Gressin, A. Guillotin, C. Guerin, L. Blanchoin, A. Michelot, Architecture dependence of actin filament network disassembly, *Curr. Biol.* 25 (2015) 1437–1447.
- [36] S. Yeoh, B. Pope, H.G. Mannherz, A. Weeds, Determining the differences in actin binding by human ADF and cofilin, *J. Mol. Biol.* 315 (2002) 911–925.
- [37] E. Kremneva, M.H. Makkonen, A. Skwarek-Maruszewska, G. Gateva, A. Michelot, R. Dominguez, et al., Cofilin-2 controls actin filament length in muscle sarcomeres, *Dev. Cell* 31 (2014) 215–226.
- [38] E. Nishida, Opposite effects of cofilin and profilin from porcine brain on rate of exchange of actin-bound adenosine 5'-triphosphate, *Biochemistry* 24 (1985) 1160–1164.
- [39] M. Hawkins, B. Pope, S.K. Maciver, A.G. Weeds, Human actin depolymerizing factor mediates a pH-sensitive destruction of actin filaments, *Biochemistry* 32 (1993) 9985–9993.
- [40] S.M. Hayden, P.S. Miller, A. Brauweiler, J.R. Bamburg, Analysis of the interactions of actin depolymerizing factor with G- and F-actin, *Biochemistry* 32 (1993) 9994–10004.
- [41] L. Blanchoin, T.D. Pollard, Mechanism of interaction of *Acanthamoeba* actophorin (ADF/cofilin) with actin filaments, *J. Biol. Chem.* 274 (1999) 15538–15546.
- [42] M.F. Carlier, V. Laurent, J. Santolini, R. Melki, D. Didry, G.X. Xia, et al., Actin depolymerizing factor (ADF/cofilin) enhances the rate of filament turnover: implication in actin-based motility, *J. Cell Biol.* 136 (1997) 1307–1322.
- [43] M.F. Carlier, Measurement of Pi dissociation from actin filaments following ATP hydrolysis using a linked enzyme assay, *Biochem. Biophys. Res. Commun.* 143 (1987) 1069–1075.
- [44] L. Blanchoin, T.D. Pollard, Hydrolysis of ATP by polymerized actin depends on the bound divalent cation but not profilin, *Biochemistry* 41 (2002) 597–602.
- [45] I.V. Dedova, O.P. Nikolaeva, V.V. Mikhailova, C.G. dos Remedios, D.I. Levitsky, Two opposite effects of cofilin on the thermal unfolding of F-actin: a differential scanning calorimetric study, *Biophys. Chem.* 110 (2004) 119–128.
- [46] E.M. De La Cruz, How cofilin severs an actin filament, *Biophys. Rev.* 1 (2009) 51–59.
- [47] W.M. Brieher, H.Y. Kueh, B.A. Ballif, T.J. Mitchison, Rapid actin monomer-insensitive depolymerization of *Listeria* actin comet tails by cofilin, coronin, and Aip1, *J. Cell Biol.* 175 (2006) 315–324.
- [48] B.L. Goode, J.J. Wong, A.C. Butty, M. Peter, A.L. McCormack, J.R. Yates, et al., Coronin promotes the rapid assembly and cross-linking of actin filaments and may link the actin and microtubule cytoskeletons in yeast, *J. Cell Biol.* 144 (1999) 83–98.
- [49] M.C. Lin, B.J. Galletta, D. Sept, J.A. Cooper, Overlapping and distinct functions for cofilin, coronin and Aip1 in actin dynamics *in vivo*, *J. Cell Sci.* 123 (2010) 1329–1342.
- [50] D. Aggeli, E. Kish-Trier, M.C. Lin, B. Haarer, G. Cingolani, J.A. Cooper, et al., Coordination of the filament stabilizing versus destabilizing activities of cofilin through its secondary binding site on actin, *Cytoskeleton (Hoboken)* 71 (2014) 361–379.
- [51] J. van Rheenen, X. Song, W. van Roosmalen, M. Cammer, X. Chen, V. Desmarais, et al., EGF-induced PIP2 hydrolysis releases and activates cofilin locally in carcinoma cells, *J. Cell Biol.* 179 (2007) 1247–1259.
- [52] K. Ohashi, K. Sampei, M. Nakagawa, N. Uchiumi, T. Amanuma, S. Aiba, et al., Damnacanthal, an effective inhibitor of LIM-kinase, inhibits cell migration and invasion, *Mol. Biol. Cell* 25 (2014) 828–840.
- [53] S.Y. Xiang, K. Ouyang, B.S. Yung, S. Miyamoto, A.V. Smrcka, J. Chen, et al., PLCepsilon, PKD1, and SSH1L transduce RhoA signaling to protect mitochondria from oxidative stress in the heart, *Sci. Signal.* 6 (2013) ra108.
- [54] J.M. Cameron, M. Gabrielsen, Y.H. Chim, J. Munro, E.J. McGhee, D. Sumpton, et al., Polarized cell motility induces hydrogen peroxide to inhibit cofilin *via* cysteine oxidation, *Curr. Biol.* 25 (2015) 1520–1525.
- [55] B.R. Graziano, E.M. Jonasson, J.G. Pullen, C.J. Gould, B.L. Goode, Ligand-induced activation of a formin–NPF pair leads to collaborative actin nucleation, *J. Cell Biol.* 201 (2013) 595–611.
- [56] J.R. Kuhn, T.D. Pollard, Real-time measurements of actin filament polymerization by total internal reflection fluorescence microscopy, *Biophys. J.* 88 (2005) 1387–1402.
- [57] R. Jaiswal, D. Breitsprecher, A. Collins, I.R. Correa Jr., M.Q. Xu, B.L. Goode, The formin Daam1 and fascin directly collaborate to promote filopodia formation, *Curr. Biol.* 23 (2013) 1373–1379.
- [58] A.K. Wolven, L.D. Belmont, N.M. Mahoney, S.C. Almo, D.G. Drubin, *in vivo* importance of actin nucleotide exchange catalyzed by profilin, *J. Cell Biol.* 150 (2000) 895–904.